Springer

Journal of Mechanical Science and Technology 23 (2009) 2645~2651

Journal of Mechanical Science and Technology

www.springerlink.com/content/1738-494x
DOI 10.1007/s12206-009-0717-5

Optimal disk clamp design to minimize stress variation of disks in a hard disk drive †

Woochul Kim*, Woo-Sung Kim and Joseph Chang

Advanced Mecha Part, HDA (Head Disk Assembly)Group, Storage System Division, Device Solution Business, Samsung Electronics Co., Ltd., 416, Maetan-3Dong, Yeongtong-Gu, Suwon City, Gyeonggi-Do, 443-742 Korea

(Manuscript Received June 22, 2008; Revised April 30, 2009; Accepted May 27, 2009)

Abstract

To avoid disk waviness and warpage in a hard disk drive, it is desirable for the stress distribution on disks fastened to a spindle motor by a clamp to be uniform in the circumferential direction while sufficient clamping force is maintained. The objective of this work is to find a clamp configuration that minimizes the circumferential stress variation on the disks while maximizing the clamping force. Topology and shape optimization methods were employed to find the optimal clamp configuration. To facilitate the optimization problem, a model for the surface contact between the clamp and the top disk was simplified to a static model where the disk clamp and spring were connected. By incorporating the surface recess, the optimized clamp has equal stiffness in the circumferential direction, except for the four tooling hole areas. Numerical simulation confirmed that the optimized clamp reduced the stress variation by about 78% without sacrificing the clamping force; in fact, it increased the clamping force.

***Keywords*:** Disk clamp; Topology optimization; Shape optimization; HDD (Hard Disk Drive); Disk warpage; Clamping force

1. Introduction

The purpose of this study is to design a hard disk drive (HDD) disk clamp in order to obtain uniform stress distribution on a disk while maintaining the required clamping force. In a motor base assembly (MBA), magnetic disks are generally fastened to a spindle motor by a clamp and kept slip-free during non-operating shock conditions. Specifically, a high clamping force is necessary and important to avoid a disk slip event when an HDD is exposed to adverse environmental conditions such as external vibration and shock. However, this clamping force generally results in unwanted disk waviness along the inner data zone. Due to a number of manufacturing constraints inherent in the clamp design including assembly tooling guide holes, the clamp is not axisymmetric in shape. Furthermore, the stress placed on the disk by the clamp is usually not distributed evenly. Disk waviness is known to have a negative impact on head flying on disks. As a result, the key design issue for a disk clamp [1-3] is the uniform distribution of stress in the circumferential direction of the disk without loss of clamping force.

Fig. 1(a) shows a vertical section view of an MBA for a 2.5" mobile hard disk drive. As shown in the figure, the MBA includes a hub, a spacer, a disk clamp, and rotating magnetic disks. Fig. 1(b) shows a schematic illustration of a typical disk clamp. One type of disk clamp used extensively in the industry is the so-called spring-type clamp. In Fig. 1(b), an opening is formed at the center of the disk clamp for a clamp screw hole. The clamp includes a pressing portion formed along the outer circumference of the

† This paper was recommended for publication in revised form by Associate Editor Jeong Sam Han

*Corresponding author. Tel.: +82 31 200 9278, Fax.: +82 32 200 3536
E-mail address: woochul1.kim@samsung.com

disk clamp to press on the upper surface of the top disk in the vertical direction. The shaft of a spindle motor is screwed to the disk clamp through the screw hole, and four guide holes are placed in an array around the center screw hole. The four guide holes of the disk clamp allow a tool holding the spindle motor to be used so that it does not rotate while the disk clamp is screwed to the spindle motor during the assembly process.

When the disk clamp is firmly fastened to the spindle motor with high clamping force, the stress applied to the disk is not uniformly distributed in the circumferential direction because of the four guide holes. This uneven stress distribution on the disk in the circumferential direction results in disk waviness. This disk waviness, which usually appears in the inner data zone as a low-frequency repetitive run out (RRO), is highly undesirable because it often causes problems such as an increase in data error rate, track misregistration (TMR) by a poor RRO compensator, unstable head flying, and other head disk interface reliability and drive performance issues.

Therefore, the objective of this work is to find an optimal disk clamp that clamps disks as flat as possible without loss of clamping force. The design method conducted in this work consists of two parts: (A) topology optimization [4-7] of a disk clamp to minimize the circumferential stress variation on the disks and (B) shape optimization [8, 9] of a disk clamp to maximize the clamping force. To facilitate the optimization of the disk clamp, the model for the surface contact [10] between a clamp and the top disk was simplified into a static model where the disk clamp and the spring were connected. As an optimization algorithm for design variable update, sequential linear programming [11] provided by DOT is used for shape optimization while the method of moving asymptote (MMA) [12] is used for topology optimization. To confirm the performance of the optimized clamp, the disk clamp-disk-spacer-hub system was modeled and a contact analysis was performed with ANSYS [13]. When compared with a commonly available clamp, the optimized clamp exhibited considerably improved stress uniformity while maintaining high clamping force.

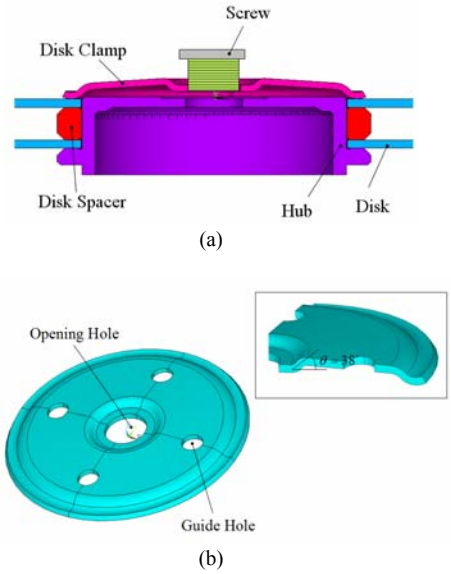

Fig. 1. (a) A cross-section view illustrating a conventional hard disk drive, (b) a schematic illustration of a conventional disk clamp.

2. Modeling of a disk clamp

When employing a structural topology optimization scheme for uniform stress distribution under the contact boundary condition, significant problems such as sensitivity analysis and convergence can occur [11-13]. The topology optimization of the three-dimensional structure under contact conditions was simplified to a static model to facilitate optimization of a disk clamp. The modeling scheme to facilitate the optimization problem is illustrated in Fig. 2(a). The contact surfaces of the clamp and the disk in the circumferential direction were connected by a set of one-dimensional elastic springs (in this work, the stiffness of a spring k_z was 10^5 N/mm) and all of the d.o.f. at the end of the springs were zero. The spring constant value of 10^3 N/mm was used because the clamping force generated was about 250N when the disk clamp was fastened by the screw at 0.25 mm in an actual experiment. The illustration in Fig. 2(b) shows the three-dimensional finite element model constructed as a baseline for the topology optimization of a disk clamp. The design domain was discretized to four-node tetra elements. The finite model was a quarter model of a circular clamp with symmetric boundary conditions along the surface edge at the angles 0° and 90°. The load was applied vertically to the lip of the opening hole. Note that this simple static modeling scheme with linear spring has been a widely used method in disk clamp design. The disk clamp was made of stainless steel (SUS). The properties of the material are given as Young's modulus

E_0=200×10^9 N/m^2, Poisson ratio ν =0.3, and density ρ_0=8000 kg/m^3.

Fig. 2(c) shows the displacement distribution of the springs in the circumferential direction. The displacement varies from a maximum value at a location along the radial direction intersecting with a guide hole to a minimum value at a location midway between guide holes in the circumferential direction. This can be explained by the fact that the stiffness is decreased due to the guide hole. The difference between the maximum and minimum displacements in the direction of z was 1.21×10^{-6} m. In the following work, we considered adjusting the displacement to the desired level instead of handling the stress between the clamp and a disk by employing topology and shape optimization.

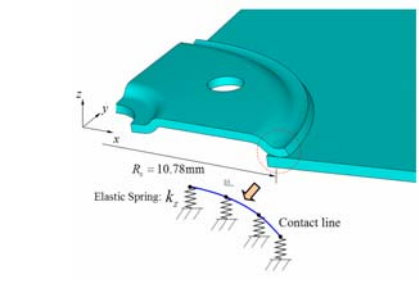

(a)

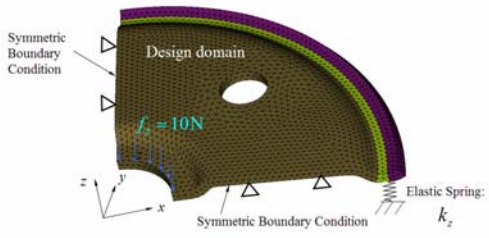

(b)

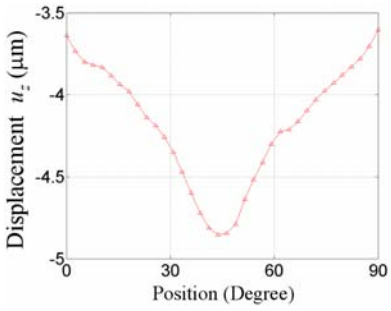

(c)

Fig. 2. (a) Modeling by one-dimensional springs at the contact surface, (b) the three-dimensional finite element model used to find a clamp configuration by topology optimization, (c) stress distribution in the circumferential direction of a disk.

3. Topology optimization of a disk clamp

Since the implementation of topology optimization for structural systems can be found in other published works [4-7], a detailed numerical procedure will not be given here. However, the underlying procedures will be briefly described. Topology optimization is a design process utilized to determine the optimal material distribution of a design domain. For topology optimization, the material status of the eth finite element was represented by a real-valued design variable ρ_e ($0 \le \rho_{\text{Lower}} \le \rho_e \le 1$) (for e=1,…, N_D, N_D: the total number of the elements in the design domain). The element with $\rho_e \approx 1$ indicated the presence of material while the element with $\rho_e \approx 0$ indicated that there was no material. If an optimal distribution of ρ_e's with a converged value of either $\rho_e \approx 0$ or $\rho_e \approx 1$ was determined, an optimal disk clamp layout could be identified. The mechanism to push ρ_e to either $\rho_e \approx 0$ or $\rho_e \approx 1$ was included in the topology optimization formulation.

3.1 Topology optimization formulation

To minimize the decrease in stiffness of the disk clamp according to a reduction of the displacement variation at the contact points, we define the objective function as the mean compliance and the constraint imposed on the displacement to achieve the desirable displacement variation level.

$$\underset{\boldsymbol{\rho}}{\text{Min}}\ W(\boldsymbol{\rho}) = \mathbf{U}^T(\boldsymbol{\rho})\mathbf{K}(\boldsymbol{\rho})\mathbf{U}(\boldsymbol{\rho}) = \sum_{e=1}^{N_D} \mathbf{u}_e^T \mathbf{k}_e(\boldsymbol{\rho})\mathbf{u}_e \quad (1a)$$

$$\text{Subject to}\quad h(\boldsymbol{\rho}) = \sum_{e=1}^{N_D} \rho_e v_e - M_c \le 0 \quad (1b)$$

$$u_z^{\text{Lower}} \le {}^i u_z^s \le u_z^{\text{Upper}},\ i = 1,2,...,N_s \quad (1c)$$

$$\mathbf{K}(\boldsymbol{\rho})\mathbf{U}(\boldsymbol{\rho}) = \mathbf{F} \quad (1d)$$

$$\boldsymbol{\rho} = \left\{\rho_1, \rho_2, ..., \rho_{N_D}\right\} \quad (1e)$$

where Σ is the assembly operator. The mass constraint is represented by h ($\boldsymbol{\rho}$). M_c is the prescribed mass and v_e is the eth element volume. The symbols $\mathbf{U}$ and $\mathbf{F}$ denote the global displacement and force vector, respectively; $\mathbf{K}$ is the global stiffness matrix; $\mathbf{u}_e$ and $\mathbf{k}_e$ are the element displacement vector and stiffness matrix, respectively; ${}^i u_z^s$ denotes the ith displacement of springs in the direction of z; N_s is the

total number of springs; and u_z^{Lower} and u_z^{Upper} are the lower and upper limit values of a displacement, respectively.

Since the element status must be controlled by ρ_e at the end of an optimization iteration, the density design variable ρ_e was assigned to each finite element along with the Young's modulus E_e. These were parameterized in each finite element with penalization using Solid Isotropic Material with Penalization (SIMP) [4, 5] as

$$E_e = \rho_e^n E_0 \quad \text{for} \quad e = 1, \cdots, N_D \tag{2}$$

where n is the penalization parameter (the value of n=3 was used in this study).

3.2 Sensitivity analysis

It was necessary to calculate the sensitivity of the objective W and the mass constraint h with respect to the design variables because we used a gradient-based optimization as the method for moving asymptotes [12],* for the topology optimization.

$$\frac{\partial W}{\partial \rho_e} = -\mathbf{u}_e^T \frac{\partial \mathbf{k}_e}{\partial \rho_e} \mathbf{u}_e \tag{3}$$

$$\frac{\partial h}{\partial \rho_e} = v_e \tag{4}$$

The sensitivity of the displacement u_i^s with respect to design variable ρ_e can be calculated as

$$\begin{aligned} \frac{d\,{}^i u_z^s}{d\rho_e} &= \frac{\partial\,{}^i u_z^s}{\partial \rho_e} + \frac{\partial\,{}^i u_z^s}{\partial \mathbf{U}} \frac{\partial \mathbf{U}}{\partial \rho_e} = \frac{\partial\,{}^i u_z^s}{\partial \rho_e} + \mathbf{L}^T \frac{\partial \mathbf{U}}{\partial \rho_e} \\ &= \frac{\partial\,{}^i u_z^s}{\partial \rho_e} + \mathbf{L}^T \mathbf{K}^{-1} \left(-\frac{\partial \mathbf{K}}{\partial \rho_e} \mathbf{U} \right) \end{aligned} \tag{5}$$

where $\mathbf{L}^T$ is a vector consisting of zeros except for the position i, corresponding to the d.o.f. of the output direction where its value is one.

To avoid the matrix inversion $\mathbf{K}^{-1}$, the adjoint variable method can be used. If the adjoint variable $\boldsymbol{\lambda}$ satisfying the following equation is determined,

$$\mathbf{K}\boldsymbol{\lambda} = \mathbf{L} \tag{6}$$

Eq. (5) can be replaced by

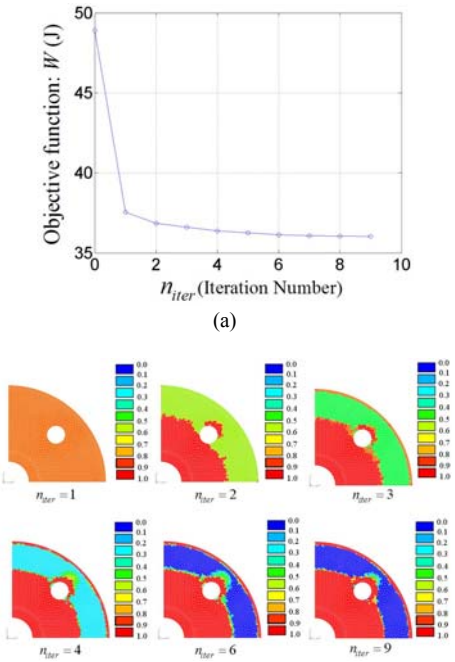

(a)

(b)

Fig. 3. (a) Iteration history of the objective function (W), (b) the intermediate and final disk clamp (n_{iter}: iteration number of the topology optimization).

$$\frac{d\,{}^i u_z^s}{d\rho_e} = \frac{\partial\,{}^i u_z^s}{\partial \rho_e} - \boldsymbol{\lambda}^T \frac{\partial \mathbf{K}}{\partial \rho_e} \mathbf{U} \tag{7}$$

3.3 Optimization results

The following list summarizes the numerical data used for the present topology optimization.

- N_D=15,600 (the number of design variables)
- N_S=36 (the number of springs)
- ρ_e at the initial iteration (e=1,…,N_D) = 0.85
- $u_z^{\text{Lower}} = -4.2\times10^{-6}$ m, $u_z^{\text{Upper}} = -4.0\times10^{-6}$ m
- M_c=0.85M_0 (M_0 = total mass of active design domain with $\rho_0 = 1$ for all elements)

The selected mass constraint ratio M_c/M_0 of 85% is used for reaching the desirable displacement variation level. In Fig. 2(c), the range for the displacement of a spring is $-4.85\times10^{-6}\,\text{m} \le {}^i u_z^s \le -3.64\times10^{-6}\,\text{m}$, we therefore used $u_z^{\text{Lower}} = -4.2\times10^{-6}$ m and $u_z^{\text{Upper}} = -4.0\times10^{-6}$ m for a more uniform displacement distribution than the conventional clamp in Fig. 1(b).

The red and blue levels within the design domain in Fig. 3 correspond to the value of the design variable ρ_e ($0 \le \rho_e \le 1$). At the end of the optimization iterations, the status of steel and no material corre-

* The authors appreciate Prof. Svanberg's help for providing his MMA code.

sponding to ρ_e =1 (red) and ρ_e =0 (blue) were reached.

The final result has the stiffest structure satisfying the permitted displacement range of Eq. 1(c). The surface of the disk clamp is recessed by 0.1 mm, except for the four tooling hole areas as shown in Fig. 3. This material distribution offers equal stiffness in the circumferential direction and results in uniform stress distribution to the contact surface of the disk.

4. Shape optimization of a disk clamp

The optimized result of Fig. 3 has uniform displacement distribution in a disk due to equal stiffness in the circumferential direction, but this result decreases the clamping force. If an insufficient clamping force is applied to a disk, disk slip may occur when a mechanical impact is received. For this reason, shape optimization of the disk clamp was carried out to maximize the clamping force. In the present shape optimization, the objective function is defined as the total clamping force without considering the effect of the four holes. Hence, the disk clamp can be assumed to be an axisymmetric shell element. The optimization problem was defined as follows;

$$\text{Maximize: } f_z^r(\mathbf{x}) \tag{8a}$$

$$\mathbf{x} = \{x_1, x_2, \ldots, x_{NP}\}, \text{ and } x_i^{\text{Low}} \le x_i \le x_i^{\text{High}}, \quad (i = 1, 2, \ldots, NP) \tag{8b}$$

where f_z^r is the reaction force at the contact node, and $\mathbf{x} \in \mathbb{R}^{NP}$ is the shape design variable vector that consists of the coordinates of shape interpolation points.

Fig. 4(a) illustrates the interpolation points chosen for the present shape optimization. The disk clamp was modeled using a B-spline curve with six control points p_i as shown in Fig. 4(a). The method given in Ref. [9] is employed for the present shape optimization. Axisymmetric finite elements are used for disk clamp discretization. Each interpolation point in the figure, except for those lying on the boundaries, has two design variables (horizontal radial and vertical coordinates). Piecewise cubic spline curves having the second-order derivative continuity are used to interpolate the disk clamp shape. The shape design sensitivities [8, 14, 15] of each of these design variables are calculated by the central finite difference method (CFDM). The shape optimization was carried out by Sequential Linear Programming (SLP) [11].

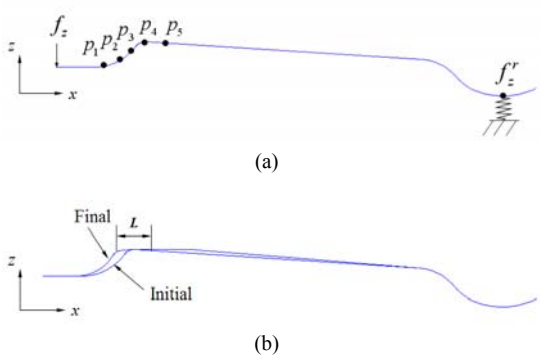

Fig. 4. (a) Definition of control points for shape optimization of a disk clamp, (b) initial and final shape of a disk clamp.

Fig. 5. Schematic illustration of the optimized disk clamp.

The initial and final shapes are shown in Fig. 4(b). Based on the disk clamp optimization results, the final shape layout of the optimized disk clamp considering manufacturability is shown in Fig. 5. In comparison with the conventional clamp shape of Fig. 2(b), the slope (θ) increased from 38° to 48° and the flat surface (L) increased to compensate for the loss of clamp force through the aforementioned topology optimization scheme.

5. Numerical verification

To confirm the superior performance of the optimized clamp, we conducted a contact analysis [10] with ANSYS [13]. At the same time, the geometrical nonlinearity [16] was taken into account in an elastic deformation analysis. The three-dimensional model of the disk clamp-disk-spacer-hub system is shown in Fig. 6. The elements used were CONTACT173, TARGET 170, and SOLID 45. The material used for the spacer and hub was aluminum while glass was

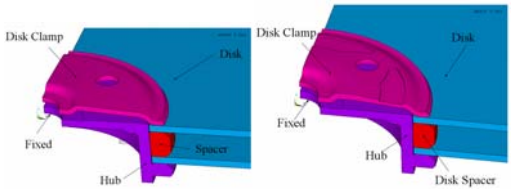

(a) (b)

Fig. 6. Finite element modeling for contact analysis: (a) a conventional disk clamp-disk-spacer-hub system, (b) the optimized disk clamp-disk-spacer-hub system.

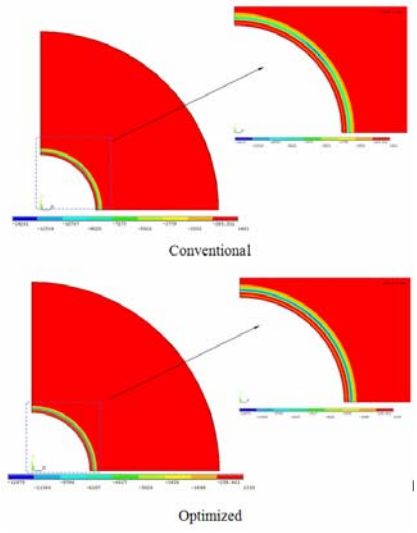

(a)

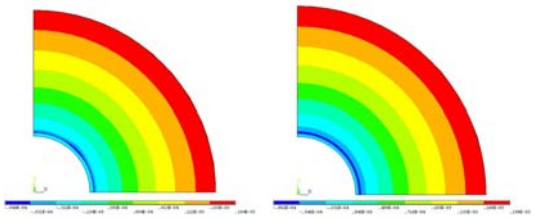

(b)

Fig. 7. Stress and displacement distribution with the optimized clamp and the conventional clamp for (a) σ_z and (b) u_z.

used for the disk. The nodes around the opening hole were given as u_z=0.25 mm for the displacement boundary condition. The friction between two bodies was obtained from the frictional coefficients table for some common materials and its value was 0.1. The illustrations in Figs. 7(a) and 7(b) show stress (σ_z) and displacement (u_z) distributions when the conventional and optimized clamps were used, respectively. It can be seen that the stress distribution of the optimized clamp was more uniform than that of the conventional clamp along the circumferential direction. Fig. 8(a) shows a comparison of the stress distribution where the stress acts on the ID (contact radius: 10.78 mm) of the disk in the circumferential direction. The average stress $\bar{\sigma}_z$ was -11.73×10^3 kN/m^2, and the relative difference $|(\sigma_z)_{\max} - (\sigma_z)_{\min}|$ was 0.36×10^3 kN/m^2 when the conventional clamp was used. When the optimized clamp in Fig. 5 was used, the average stress $\bar{\sigma}_z$ was -12.51×10^3 kN/m^2; the difference was reduced by 78%. These results show that the optimized clamp had a more effective stress distribution while maintaining a higher clamping force than the conventional clamp. To investigate disk waveness, the displacements at the disk radius (D_r=32.5 mm) were plotted as shown in Fig. 8(b). It can be seen that the optimized clamp is a structurally more balanced design compared to a conventional clamp design because it minimizes warpage of the disk upon contact. Moreover, the stress applied to the disk is evenly distributed in the circumferential direction. Consequently, the optimal surface recess of a disk clamp to equal stiffness in the circumferential direction significantly improved the stress uniformity by as much as

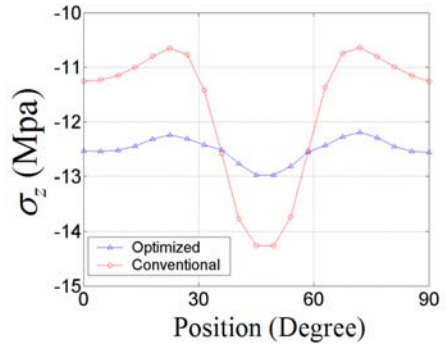

(a)

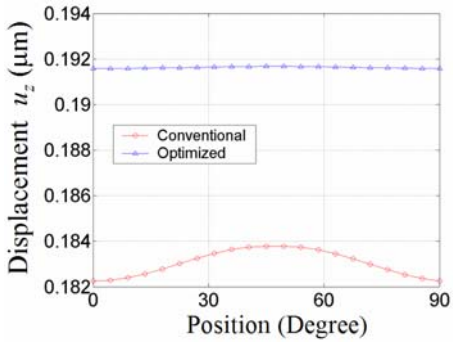

(b)

Fig. 8. (a) Comparison of the stress distribution of σ_z, (b) comparison of the displacement distribution of u_z.

about 78%.

6. Conclusion

For reliable and accurate read and write performance on the inner data zone of a hard drive, disk waviness should be minimized when disks are secured to a motor by a clamp. This investigation concerned a clamp configuration that minimizes stress variation in the circumferential direction of a disk while sustaining the required clamping force. By employing topology and shape optimizations, an optimized clamp with surface recess, except for the four tooling hole areas, was obtained. With this structural configuration, equal stiffness was generated in the circumferential direction, resulting in uniform stress distribution on the disk at contact without sacrificing any significant clamping force. Numerical simulation showed that the stress variation on a disk by the optimized clamp was improved by 78% in comparison with that of a commonly used disk clamp with high clamping force.

Reference

[1] H. S. Lee, J. S. Koh, T. Y. Hwang and W. C. J, Optimal design of disk clamp to reduce RRO in a hard disk drive, *Proceeding of the Korean Society of Noise and Vibration Engineering Conference* (2002) 539-542.

[2] A. M. Lindrose, Disk clamp with contoured peripheral wall height, *US patent*, No. 5880906 (1999).

[3] H. S. Lee, J. S. Koh, T. Y. Hwang and W. C. J, Disk clamp of hard disk drive, *US patent*, No. 0012882 A1 (2004).

[4] M. P. Bendsoe and O. Sigmund, *Topology Optimization-Theory, Methods and Applications*, Springer-Verlag, Berlin Heidelberg New York, (2003).

[5] G. H. Yoon and Y. Y. Kim, Topology optimization of material-nonlinear Continuum structures by the element connectivity parameterization, *Int. J. Num. Meths. Eng, March*. 69 (2007) 2196-2218.

[6] J. Yoo and H. J. Soh, An optimal design of magnetic actuators using topology optimization and the response surface method, *Microsystem Technologies* 11 (12) (2005) 1252-1261.

[7] W. Kim, J. E. Kim, and Y. Y. Kim, Coil configuration design for the Lorentz force maximization by the topology optimization method: applications to optical pickup coil design, *Sens. Actuators A* 121 (2005) 221-229.

[8] S. Wang and J. Kang, Shape Optimization of BLDC Motor Using 3-D Finite Element Method, *IEEE Transaction on Magnetics* 36 (4) (2000) 1119-1123.

[9] Y. Ding, Shape optimization of structures–a literature survey, *Comput. Struct*. 24 (6) (1986) 985-1004.

[10] P. Wriggers, *Computational Contact Mechanics*, Wiley, New York, (2002).

[11] E. J. Haug, K. K. Choi and V. Komkov, *Design sensitivity analysis of structural systems*, Academic Press, New York, (1986).

[12] K. Svanberg, The method of moving asymptotes-a new method for structural optimization, *Int. J. Numer. Mech*. 24 (1987) 359-373.

[13] ANSYS, *ANSYS Low-frequency Electromagnetic Analysis Guide ANSYS*, Inc., Canonsburg, PA (2003).

[14] S. Wang and S. H. Ki, Configuration design sensitivity analysis using CAD-based design velocity field*, Proc. of 2nd World Congress of Structural and Multidisciplinary Optimization* (1997) 265-270.

[15] J. S. Arora, *Introduction to optimum design*, New York, McGraw-Hill, (1989).

[16] K. J. Bathe, *Finite element procedures*. Prentice hall: New Jersey, (1996).

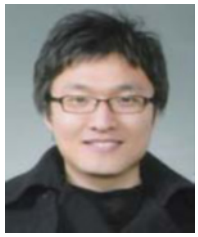

Woochul Kim received the B.S. degree from Inha University and the M.S. and Ph.D. degrees in mechanical engineering from Seoul National University in 2007. He has been the engineer of Advanced Mecha Part in Samsung Electronics since 2007. His research interests are the design optimization of various magnetic systems, the topology optimization of systems requiring the coupled analysis of magnetic field and structural vibrations.